



Choudhary, T. R., Ball, D., Ramos, J. F., Stefansson, E. and Harvey, A. R. (2019)
Remote sensing of blood oxygenation using red-eye pupil reflection. *Physiological Measurement*, 40(12), 12NT01.

There may be differences between this version and the published version. You are advised to consult the publisher's version if you wish to cite from it.

<http://eprints.gla.ac.uk/206353/>

Deposited on: 21 April 2020

Enlighten – Research publications by members of the University of Glasgow
<http://eprints.gla.ac.uk>

1
2
3
4
5
6
7
8
9
10
11
12
13
14
15
16
17
18
19
20
21
22
23
24
25
26
27
28
29
30
31
32
33
34
35
36
37
38
39
40
41
42
43
44
45
46
47
48
49
50
51
52
53
54
55
56
57
58
59
60

Remote sensing of blood oxygenation using red-eye pupil reflection

Tushar R. Choudhary^{*,1,2}, Derek Ball⁴, Javier Fernandez Ramos², Einar Stefansson³, Andrew R. Harvey²

¹ The Roslin Institute and Royal (Dick) School of Veterinary Studies, University of Edinburgh, Edinburgh, Midlothian, EH25 9RG. United Kingdom.

² School of Physics and Astronomy, University of Glasgow, Glasgow, U.K.

³ University of Iceland, Landspítali - The National University Hospital of Iceland

⁴ Institute of Medical Education in Medical and Dental Sciences, University of Aberdeen, Aberdeen, UK

* Corresponding Author

Keywords: Optical density ratio, spectral imaging, choroid, oxygen

Abstract

We describe a new method to non-invasively sense the oxygen saturation of choroidal blood at stand-off using bilateral images of the pupils. This provides a proxy for remote sensing of cerebral and systemic blood oxygenation. A modified fundus camera, fitted with an Image Replicating Imaging Spectrometer (IRIS) was used to record snapshot spectral images at eight different wavelengths in a single exposure of light reflected from the ocular fundus and transmitted through the pupils. Light intensities at two infrared wavelengths, 780 nm and 800 nm (oxygen sensitive and isosbestic) were used to calculate the optical density ratio (ODR) of the images. A pilot study on ten healthy human subjects was conducted where spectral images of the pupil reflection were recorded under conditions of inspired room air (normoxia) and air containing 15% oxygen (mild hypoxia) while simultaneously measuring oxygen saturation by pulse oximetry. A significant reduction ($P < 0.001$) in ODR of the two images was observed during hypoxia and the ODR returned to baseline on resumption of normoxia. We demonstrate that measurement of the choroidal ODR can be used as a method to detect changes in blood oxygenation that correlate positively with pulse oximetry and with a noise-equivalent oximetry precision of 0.5%. The described technique has the potential to be used remotely and non-invasively to assess changes in oxygen metabolism and status.

1. Introduction

The retina has a particularly high metabolic demand for oxygen, which that is met mainly by the choroid (about 85%) with the retinal circulation providing the remaining 15%[1, 2]. The choroid supplies the outer layers of the retina including the photoreceptors while the inner layers of the retina, including the retinal ganglion cells, are supplied by the retinal vessels. The choroid is supplied with blood by the ophthalmic artery, which is a branch of the internal carotid artery, and as such is considered to be a part of the cerebral vasculature[3]. Choroidal

1
2
3 37 vessels (arteries and venules) have a very high oxygen tension and a very low arteriovenous
4
5 38 oxygen saturation difference, in the region of about 3% [4]. It is possible, with traditional
6
7 39 spectrophotometric methods, to assess and study oxygen saturation in retinal vessels non-
8
9 40 invasively [5-8] or invasively through the application of phosphor into the circulation [9, 10]
10
11 41 or direct measurement through the use of an oxygen electrode[11]. We report a technique that
12
13 42 operates at standoff and non-invasively and so offers particular advantages as a technique for
14
15 43 routine sensing of choroidal oxygenation in humans. Our technique provides sensitive sensing
16
17 44 of blood oxygenation and can be further developed for measurement of absolute oximetry. Few
18
19 45 studies on choroidal oxygenation have been reported and those that have are restricted mainly
20
21 46 to animal studies [12]. Due to the close coupling between cerebral and choroidal vasculature,
22
23 47 measurement of choroidal oxygenation would provide a surrogate measure of oxygen
24
25 48 saturation of the cerebral vasculature. In terms of retinal diseases, choroidal oximetry could
26
27 49 prove to be useful in understanding pathophysiology of diseases like age-related macular
28
29 50 degeneration [13, 14], diabetic retinopathy [15-17] and be employed as a useful diagnostic tool
30
31 51 for Alzheimer's disease risk [18, 19] in which cerebral blood flow plays an important role.
32
33
34
35
36
37

38 52 The first non-invasive measurement of choroidal oxygen saturation was demonstrated by
39
40 53 Broadfoot et al [20] in 1961, using a modified Gullstrand ophthalmoscope to focus light
41
42 54 reflected from the human ocular fundus onto a photomultiplier. Light was time-sequentially
43
44 55 spectrally filtered using a filter wheel with red and cyan colour filters. The study reported that
45
46 56 the fundus reflection of red light changed significantly when the choroidal oxygenation was
47
48 57 altered in subjects breathing nitrogen or by apnea. Laing et al employed non-imaging fundus
49
50 58 reflectometry at wavelengths of 650 nm and 805 nm to determine the oxygen saturation in the
51
52 59 choroidal blood [21] for subjects with acute mild hypoxia induced by breathing a hypoxic-air
53
54 60 mixture. More recently, Kristjandottir et al [22] imaged oxygen saturation in choroidal vessels
55
56 61 based on images recorded at wavelengths of 570 nm and 600 nm using a modified fundus
57
58
59
60

1
2
3 62 camera. The study was however, restricted to subjects with very low pigmentation that
4
5 63 provided sufficient visibility of the choroidal vessels within the retinal images and at the visible
6
7 64 wavelengths suitable for vascular oximetry. Fundus reflection has also been used to quantify
8
9 65 retinal pigments, including macular pigment [23] and melanin [24, 25] as well as to study
10
11 66 diseases and treatment efficacy; for example, in diabetes [26] and glaucoma [27, 28]. A review
12
13 67 of fundus reflection characterisation and its application is presented in [29]. We report here a
14
15 68 proof-of-concept demonstration of a new technique for remote assessment of SpO₂ based upon
16
17 69 reflection of light from the pupil. This is the ‘red-eye’ effect familiar from routine flash-
18
19 70 illuminated photography of faces. It offers oximetry without contact, and in principle at
20
21 71 considerable range, that could be applied, for example, for remote triage in emergency care or
22
23 72 where conventional pulse oximetry is not possible. The red-eye effect is due to light that has
24
25 73 been transmitted into the pupil, and undergoes a two-way transmission through the retinal and
26
27 74 choroidal tissue and is reflected by the sclera at the back of the eye.
28
29
30
31
32
33

34 75 The aim of this proof of concept study was to demonstrate the feasibility of remote sensing of
35
36 76 choroidal oxygenation using spectral images of the pupil reflection. We accomplished this by
37
38 77 calculation of spectral optical density ratios of pupil reflections under conditions of normoxia
39
40 78 and during a period of inhaling a hypoxic gas mixture. We hypothesised that the changes in
41
42 79 optical density ratio, as a function of normoxia and hypoxia, would mirror the simultaneously
43
44 80 measured changes in systemic oxygenation determined from finger pulse oximetry.
45
46
47

48 81 **2. Methods**

50
51
52 82 *2.1 Physical principles of oximetry using pupil red-eye reflection:* In the absence of
53
54 83 illumination, the eye pupil appears dark, but with bright illumination from a source located
55
56 84 close to the point of observation, as is common in flash photography, pupils appear red due to
57
58 85 the interaction of light with blood in the ocular fundus. At wavelengths in the region 500-
59
60

600nm this reflection is due mainly to bulk optical scattering and reflection from within the retina. At wavelengths between 630 and 800nm, where the optical transmission of blood is much higher, a significant fraction of light is transmitted through the retina and choroid and is reflected by the sclera. At these longer wavelengths, it is the spectral variation in the absorption of light by choroidal blood that dominates the spectrum of the red-eye reflection: the absorption by the photoreceptor layer and nerve-fibre layers in the retina is typically less than about 2% at these wavelengths [30] and does not have a significant impact on our measurements. There is however absorption of light by melanin in the pigment epithelium layer and within the choroids, which correlates with eye and skin pigmentation of the subject and does affect measured optical densities.

The choroid has an extremely dense vasculature and at about 400 μm thick is much thicker than the retina and therefore is the dominant determinant to the spectrum of the pupil reflection in the 630-800 nm range. The technique presented here exploits the spectral variation in the absorbance coefficients of oxyhaemoglobin and deoxyhaemoglobin; that is, the same principle on which retinal oximetry is based. The spectrum of light reflected from the choroid is dependent upon blood-oxygen saturation and the relevant fractions of oxy- and deoxyhaemoglobin. As for two-wavelength retinal oximetry, using one isosbestic wavelength and one oxygen-sensitive wavelength to record choroidal reflection, the oxygen saturation of choroidal blood can be characterised.

The geometry for imaging and illumination of the eye and the gaze angle determine the characteristics of the brightness and spectrum of the fundus reflection. In conventional photography of faces, red-eye fundus reflection is avoided (for aesthetic reasons) by displacement of the flash illumination from the camera lens so that the area of the retina illuminated by the flash lamp has zero or reduced overlap with the area of the retina that is

1
2
3 110 geometrically visible from the position of the camera lens. We have employed a conventional
4
5 111 fundus camera for which the illumination and imaging optics are coaxial leading to a high
6
7
8 112 degree of overlap between the illuminated and visible areas of the fundus so as to enhance the
9
10 113 intensity of light returned through the pupil.
11
12
13 114 For spectral imaging of the oximetric fundus reflection, the fundus-camera was moved from
14
15 115 its usual position for imaging through the pupil; with the objective lens about 40 mm from the
16
17 116 eye; to a new position of 90 mm away so as to increase the field of view and enable
18
19 117 simultaneous snapshot spectral imaging of both pupils as can be seen from the images in Figure
20
21
22 118 1.
23
24
25 119 The illumination and image formation is illustrated by the optical ray-trace shown in the upper
26
27 120 image in Figure 2. This was calculated using the *Zemax*© optical design programme and
28
29 121 employing a schematic model for the human eye as reported in [31]. As is conventional for a
30
31 122 mydriatic fundus camera the light is focused to an annulus with an external diameter of 6 mm
32
33 123 located 40 mm from the front objective lens. During conventional imaging of the retina, this
34
35 124 annulus is positioned within the pupil and a glare-free image of the retina is recorded through
36
37 125 the dark non-illuminated centre of the annulus. The emmetropic eye is naturally focused at
38
39 126 infinity (mydriasis is used in our experiments) and so the image plane of the illumination
40
41 127 annulus is about 10 mm behind the retina and a blurred image of the annulus is formed at the
42
43 128 retina. From the ray-traced model, we determined that the blurred image of the illumination
44
45 129 annulus has a diameter of 4.4 mm at the retina, however lateral diffusion of light results in a
46
47 130 significantly wider disk being illuminated. We employed ray tracing to simulate how
48
49 131 illumination by the retinal illumination affects the image formed of the pupil by the retinal
50
51 132 camera. This showed that a disc of 6.6 mm at the retina contributes to the imaged pupil
52
53 133 radiance, which we call the imaged-pupil radiance (IPR) disc. The approximate relative
54
55 134 dimensions of the illumination and IPR discs are depicted by the orange and blue discs
56
57
58
59
60

superimposed on a typical retinal image in Figure 2. At these infrared wavelengths, the tissue point-spread function of the retina is quite large, between 1-2 mm, effectively blurring and expanding the illumination disc on the retina to fill the IPR disc. It is apparent from Figure 2 that the pupil radiance image is determined by the integral of the light scattered from within the IPR disc and will therefore be expected to vary homogeneously across the pupil, but will be increased when the optic disc (which has a high albedo) falls within the IPR disc leading to localised brightness spots within the pupil image. Thus, when the subject fixates on the illumination point, the IPR disc is centred on the macula and the image of the pupil is determined by two-way transmission of light through the macula and surrounding retina, through the choroid to the sclera, enabling high-quality choroidal oximetry. If the direction of gaze is turned nasally however, the optic disk reflection contributes to the IPR disc contaminating the pupil image with scattered light and has the reduced interaction with the choroid.

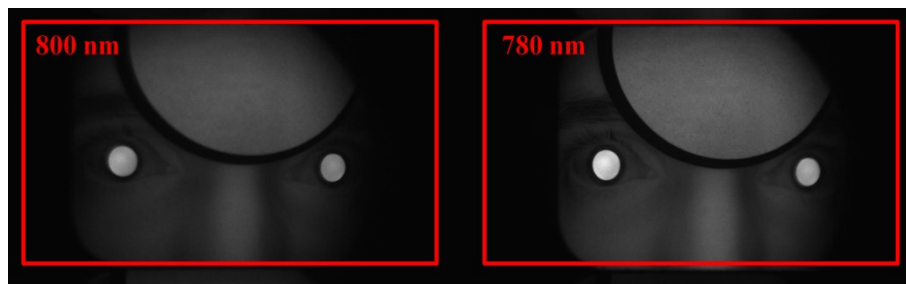


Figure 1. A spectral image of the upper face captured by IRIS system. The two pupil reflexes are visible together with a calibration tile. The two sub-images used for choroidal oximetry were 800 nm as isosbestic and 780 nm as oxygen sensitive are shown above.

To determine whether, for typical measurements, the optic disc intrudes into the IPR disc and contaminates the pupil images, the effect of the angle of gaze on fundus reflection was determined by recording fundus-reflection pupil images for two subjects as the angle of gaze was changed from an extreme nasal side to extreme temporal side as the subject tracked the

1
2
3
4
5
6
7
8
9
10
11
12
13
14
15
16
17
18
19
20
21
22
23
24
25
26
27
28
29
30
31
32
33
34
35
36
37
38
39
40
41
42
43
44
45
46
47
48
49
50
51
52
53
54
55
56
57
58
59
60

fundus-camera fixation light. The fundus ODR was calculated for five images at each angle of gaze. The effect of angle of gaze on ODR is presented in section 3.1.

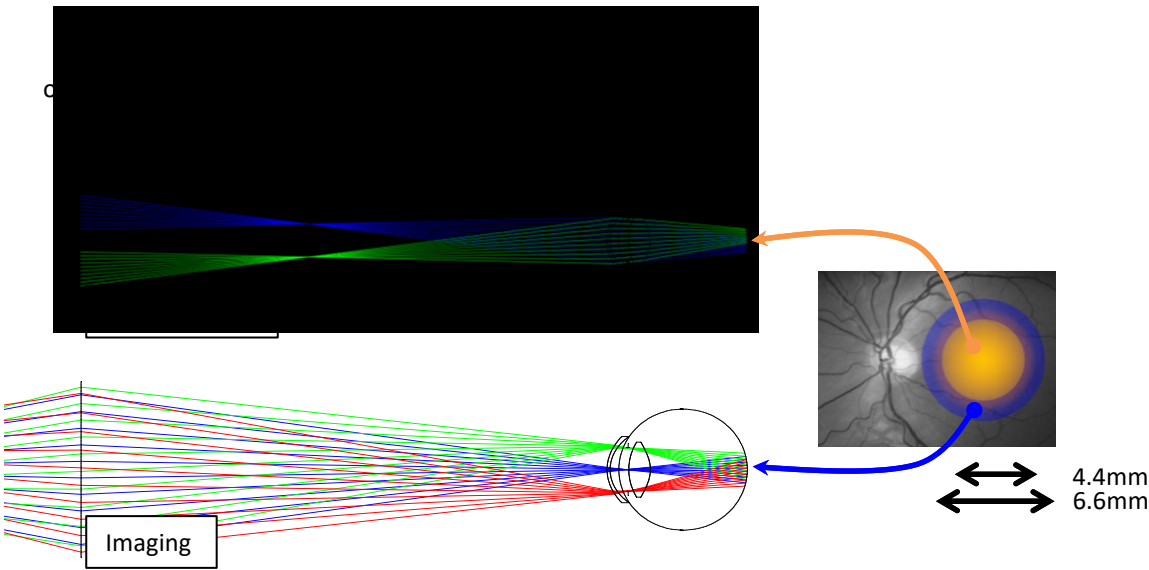


Figure 2. Optical ray-trace of the illumination of the retina by the fundus camera for an emmetropic eye (upper ray trace) and of the fundus contributing to the radiance imaged at the pupil (lower ray trace). The inset image depicts the illumination (blue) and reflex (orange) discs superimposed on an image of a typical retina and centred on the macula.

2.2 Imaging Setup: Spectral images were acquired using a modified commercial fundus camera (Topcon TRC 50 IA, Japan) fitted with an image-replicating imaging spectrometer (IRIS), (see Figure 3), which acquires images in a single snapshot at eight wavelengths optimised for oximetry [32-36], IRIS consists of a cascade of two-beam polarising interferometers that simultaneously spectrally filter and replicate images to yield, in this case, eight narrowband images onto a single detector array. Interferometric spectral filtering by IRIS provides the well-known Fellgett multiplex advantage of two-beam interferometry [37] enabling the highest possible signal-to-noise ratios to be attained with the limited optical intensities that can be safely used with the eye. We employed an IRIS system for which the waveplates had been optimised for retinal vascular oximetry, providing isosbestic and oxygen-sensitive spectral bands in the region 560-605 nm. Because IRIS passbands spectrally replicate with a specific free-spectral range in a manner similar to a Fabry-Perot interferometer, it has thus been possible

to use this IRIS design for spectral imaging in the near infrared simply by the use of a different spectral bandpass filter to restrict the free spectral range to a region in the near infrared. We employed a 25 nm bandwidth band-pass filter with centre wavelength 788 nm to spectrally filter light from the fundus camera inspection lamp, restricting the measurement to the free-spectral range of IRIS for which only a single spectral transmission lobe occurs. The spectral transmission functions of the eight sub-images of this IRIS system in the wavelength range 760-850 nm are shown in Figure 3. From the eight spectrally filtered images, two images with spectral transmission peaks at 780 nm and 800 nm were employed to calculate optical density ratio. The image at 780 nm provides sensitivity to blood oxygenation and 800 nm corresponds to an isosbestic wavelength for which absorbance is approximately independent of oxygenation.

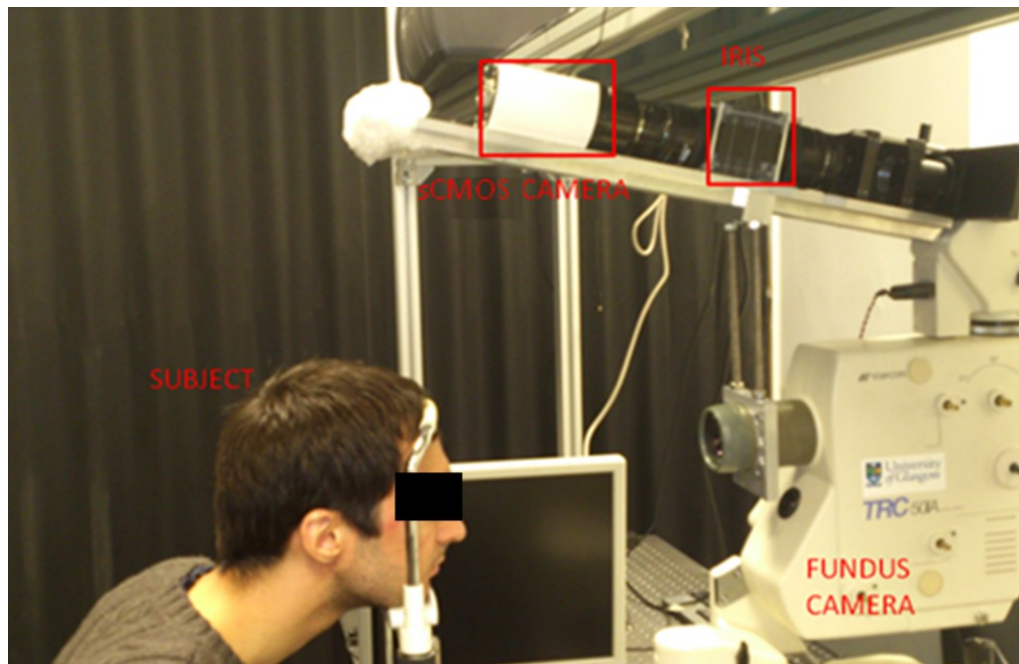


Figure 3: Experimental setup of the modified fundus camera to record the red eye pupil reflection.

The objective of the fundus camera was located 90 ± 5 mm away from the eyes of the subjects with the head stabilised using a headrest. The eyes of the subjects were illuminated with the filtered infra-red light and the spectral images of the pupils were captured simultaneously by a

sCMOS camera (Zyla, Andor; Belfast, U.K.) located to intercept the image relayed through IRIS from the image plane of the fundus camera. An example of a captured raw image is shown in Figure 1.

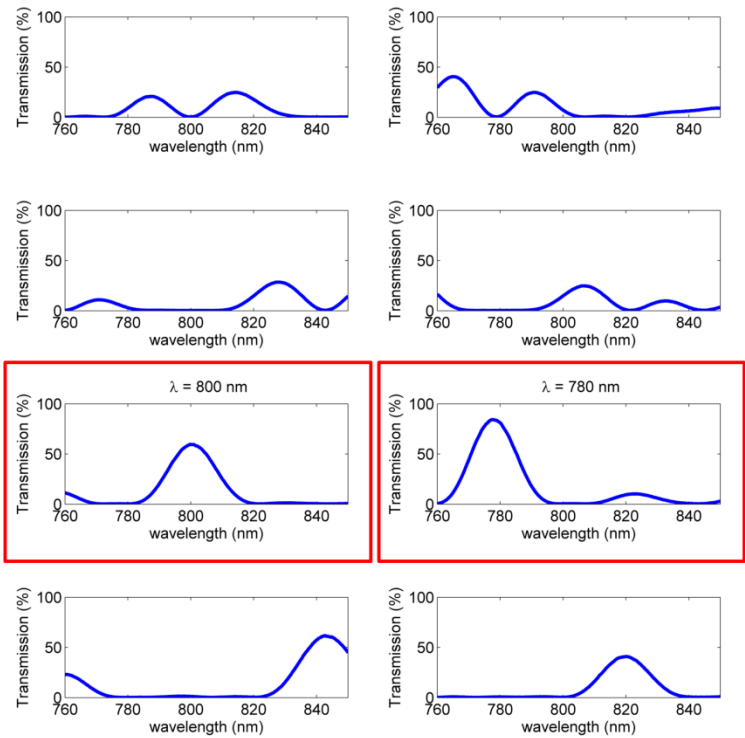


Figure 4. Spectral transmissions of 8 sub-images recorded with the IRIS imaging system. The two sub-images used for choroidal optical density ratio measurements were 800 nm and 780 nm and are highlighted in red.

2.3. Oximetric analysis:

We assume that optical attenuation of infrared light transmitted through the choroid obeys the Beer-Lambert law and therefore, as described in the appendix, the ratio of the optical densities for light transmission recorded at oxygen-sensitive and isosbestic wavelengths varies in proportion to blood oxygenation as has been demonstrated by Beach et al [38] for oximetry of the retinal vasculature. For application in the retina, the optical density of the vasculature is determined by the ratio of intensity at the centre of a blood vessel to an estimate of the reflected

light in the absence of the vessel determined by interpolation of the light on either side of the vessel. In an analogous metric, we define the optical density ratio as

$$ODR = \frac{\log_{10} R^{780}}{\log_{10} R^{800}} = \frac{\log_{10} \frac{v_p^{780}}{v_c^{780}}}{\log_{10} \frac{v_p^{800}}{v_c^{800}}} , \quad (1.0)$$

Where, $R^\lambda = v_p^\lambda / v_c^\lambda$ is the ratio of the average intensities of the images of the pupil and a calibration tile (visible in front of the forehead in Figure 1) at wavelengths $\lambda = 780$ nm and 800 nm. In the appendix we show that the ODR varies linearly with oxygen saturation of choroidal blood. At 780 nm blood becomes increasingly transparent with increasing oxygenation causing the ODR to increase. Note that the light emitted by the pupil is non-Lambertian, concentrating light towards the source and transmission, and the absorbance of the choroid is low. So the pupil image can be brighter than a unity-albedo reflector. Although both pupils can be imaged simultaneously, the results presented here are based on one pupil (right).

2.4. Fundus ODR with Changing Inspired Oxygen in Healthy Human Subjects

Ten healthy subjects were recruited to this study (eight males and two females, age 27 ± 9 years mean \pm SD;). Written informed consent was obtained from all subjects. Subjects were briefed about the experimental procedure and asked to refrain from consuming any alcohol or caffeinated drink on the day prior to the experiment. The study was approved by the Heriot-Watt University Ethics Committee. All procedures were performed in accordance with the tenets of the Declaration of Helsinki. All the subjects recruited were healthy, non-smokers, without history of a respiratory disorder and taking no medication.

On the day of study, they were again briefed about the experimental protocol. Age, sex, weight was recorded. Tropicamide (1%, Bausch & Lomb, Chauvin Pharmaceuticals, Ltd., U.K.) was

228 used to dilate the pupil. After about ten to fifteen minutes maximum dilation of the pupils,
229 typically 8 mm, was achieved and the subjects were ready to be imaged.

230 Pupil reflection images were acquired for all the subjects under normoxia (21 % inspired
231 oxygen). Hypoxia was then induced by changing the inspired oxygen to 15 % using a hypoxia
232 generator (Everest Summit II Hypoxic Generator; Hypoxico, Inc., New York, NY, USA). [39]
233 Pupil reflection images were acquired under hypoxic conditions. In total five sets of images
234 were acquired- three under normoxia and two under hypoxia (in alternating order). The
235 peripheral arterial oxygen saturation was monitored using fingertip pulse oximeter
236 (AUTOCORR; Smiths Medical ASD Inc., Rockland, MA, USA) during both normoxia and
237 hypoxia conditions. All images (normoxic and hypoxic conditions) were analysed to calculate
238 the fundus ODR. A paired t-test (SigmaPlot, Systat Software Inc.) was used to determine
239 significance of the result.

240 **3. Results**

241 *3.1. Effect of Angle of Gaze on Fundus ODR*

242 As previously discussed, it was assumed that when the subject fixates on a compact light source
243 imaged on the macula, only the choroid and retina will contribute to the fundus reflection, but
244 that some misalignment of the gaze may introduce a contribution from the optic disc and that
245 this would modify the oximetric spectral signature. To assess this potential issue the effect of
246 the angle of gaze on the pupil image was analysed in two subjects. Figure 5 shows the effect
247 of the angle of gaze on the ODR for two subjects as the angle of gaze was changed from extreme
248 temporal through to extreme nasal. The change in gaze direction corresponds to sweeping the
249 area of the fundus contributing to the pupil image from the temporal fundus, macular region,
250 optic disc to nasal side of the fundus. The elevated plateau in the ODR corresponds to angle
251 for which the reflection from the optic disc contributes and hence for which the pupil image is

both brighter and whiter. The gaze angles for which the optic-disc reflection partially contributes to the pupil image is apparent from the presence of brighter areas in a non-uniform pupil image and are thus easily identified and avoided.

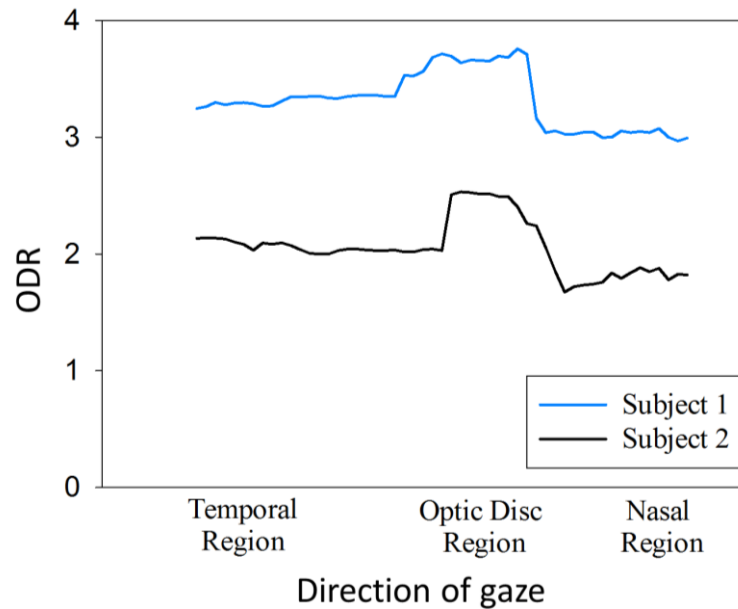
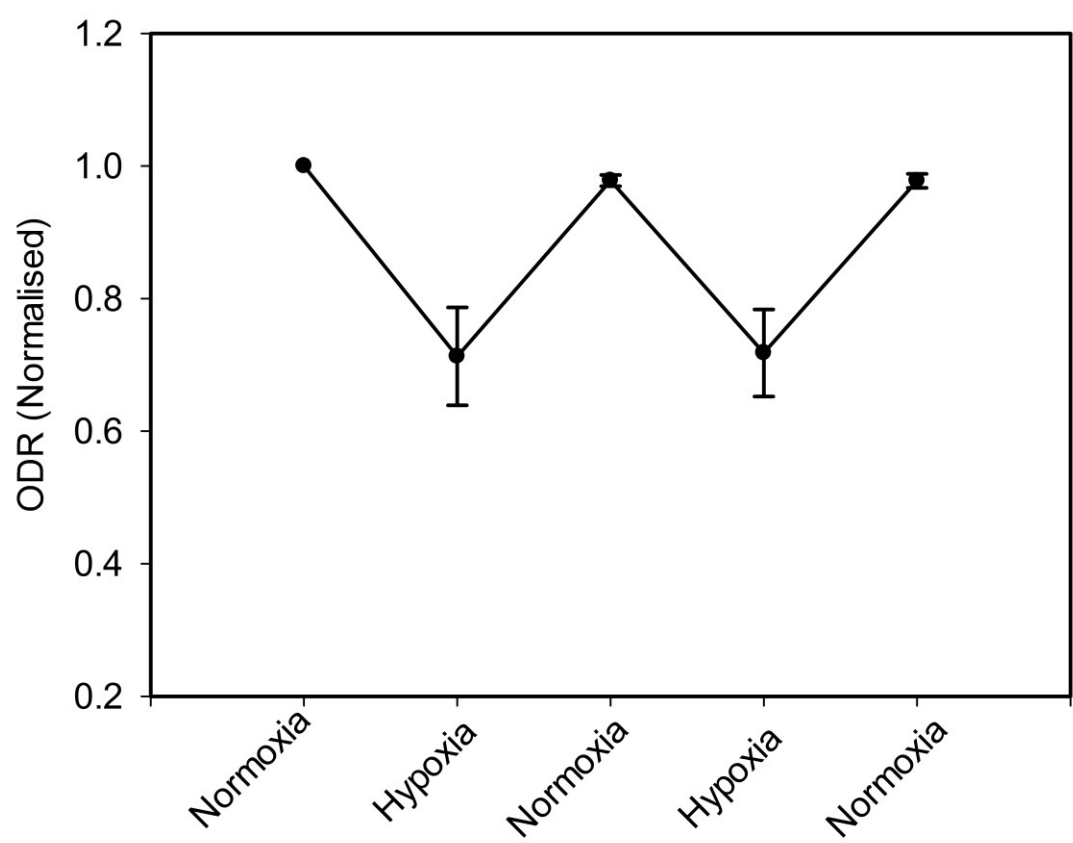


Figure 5. Variation of pupil image ODR with the angle of gaze. The high ODR plateau region corresponds to the optic disc which is closer to white than the rest of the fundus.

3.2. Fundus ODR with Change in Inspired Oxygen in Healthy Human Subjects

The variation in ODR was determined as the inspired gas was cycled between normoxic 21 % (Fraction of Inspired oxygen) FiO_2 , and hypoxic 15 % FiO_2 conditions. A pulse oximeter (AUTOCORR; Smiths Medical ASD Inc., Rockland, MA, USA) placed over the index finger throughout the experiment monitored and recorded oxygen saturation. The recorded variation in ODR (normalised with the first normoxia measurements), averaged over 2.5 normoxic/hypoxic cycles, is shown for ten subjects in Figure 6 and the variation in average ODR with pulse oximetry is shown in Figure 7. The reduction in ODR between each level of

1
2
3 267 normoxic and hypoxic FiO_2 and also with fingertip pulse oximetry is highly significant ($P <$
4
5 268 0.001 for each case).
6
7
8
9



37 269
38
39
40 270 **Figure 6.** Changes in optical density ratio (normalised) as a function of either normoxia (21 % FiO_2 , O_2 Saturation
41 271 97 %) or hypoxia (15 % FiO_2 , O_2 Saturation 86 %) in ten subjects. ODR was found to be directly proportional to
42 272 pulse oxygen saturation.
43

44 273
45
46 274
47
48
49 275
50
51
52
53
54
55
56
57
58
59
60

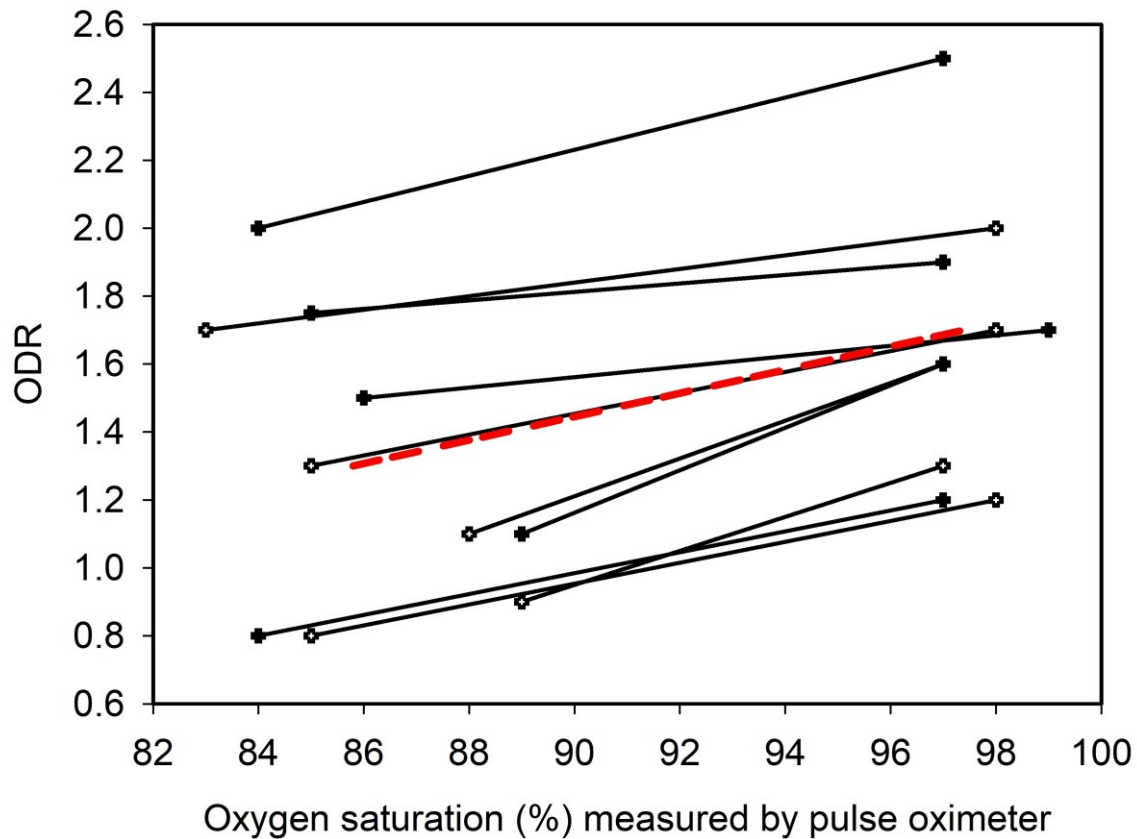


Figure 7. Oxygen saturation measured by pulse oximeter versus changes in optical density ratio in each of the ten subjects. Each black line represents one of the subjects and the red dotted line is averaged ODR of the ten subjects at hypoxia and normoxia.

The repeatability and stability of the technique was demonstrated by the temporal recordings of ODR for two subjects over a period of 60 seconds when breathing room air as shown in Figure 8, showing a root-mean-square variation of 0.019 compared to a typical modulation in ODR of 0.3: a signal-to-noise ratio of 16. The average gradient of the variation of ODR with oxygenation saturation is 3.47 and so the noise-like variations in Figure 8 correspond to noise-equivalent variations in oxygen saturation of 0.5%.

Collectively, the data in Figures 6, 7 and 8, illustrates that the decrease in ODR mirrored the effect of changing the inspired gas mixture. Measurement of choroidal ODR enabled sensing of a reduction in systemic blood oxygenation during hypoxia exposure. This observation was

supported by the pulse oximeter data and the fact that the ODR remained stable over time (60 seconds).

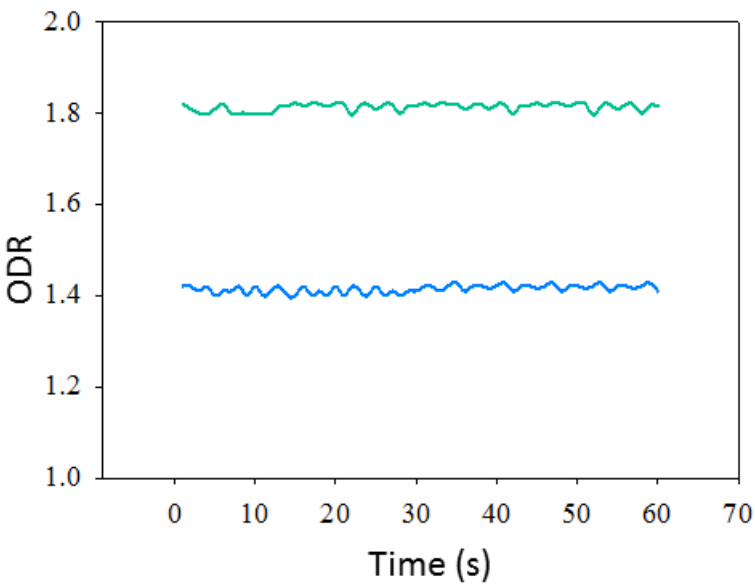


Figure 8. Pupil Optical Density Ratio for two subjects, (as indicated by green and blue lines) at room air with respect to time.

4. Discussion

In this study, a non-invasive method to sense oxygen saturation in choroidal blood is presented. The pupil ODR is sensitive to blood oxygenation and declines with a decrease in blood oxygenation, as demonstrated in human subjects breathing gas with a reduced oxygen content. The pupil ODR was assessed under normoxia in healthy human subjects and was found to decrease significantly ($P < 0.001$) when compared with the hypoxia condition. At both normoxia and hypoxia arterial blood-oxygen saturation was monitored with a finger-tip pulse oximeter. The pupil reflection was recorded simultaneously for three normoxia stages and two hypoxia stages for each subject. The fundus ODR decreased significantly between each stage

1
2
3 304 of normoxia and hypoxia (Figure 5) for all the ten subjects. The fundus ODR was also recorded
4
5 305 for 60 seconds at room air for two subjects, and was found to be stable with time (Figure 8).
6
7
8 306 The results presented in this study are comparable with the results obtained by Broadfoot[20]
9
10 307 and by Laing[21]: both studies reported a decrease in the reflection intensity with a decrease in
11
12 308 blood oxygenation. The imaging and recording setup presented here, however, is simpler and
13
14 309 has advantages over the methods used in those two previous studies [20, 21]. In their
15
16 310 experimental methodology, the imaging system comprised of a fundus camera to image the
17
18 311 eye, and an elaborate electronic system with photomultipliers and photodiodes to record the
19
20 312 intensity of the reflections from the eye. Broadfoot used a filter wheel assembly to time-
21
22 313 sequentially record the intensity at different wavelengths whereas Laing's apparatus used
23
24 314 dichroic mirrors to separate reflections at two wavelengths, which were recorded
25
26 315 simultaneously with two photodiodes. The setup presented here has a fundus camera fitted with
27
28 316 an IRIS device, which enables recording of spectral images at multiple wavelengths in a single
29
30 317 snapshot onto a single detector. The advantage of using snapshot imaging ensures that pupil
31
32 318 images at different wavelengths were captured at the same point of time thus removing any
33
34 319 variability due to a temporal difference in recordings. Our device recorded the spectral images
35
36 320 and the ODR was subsequently calculated from the images. Any eye movement was then
37
38 321 easily corrected by image registration to enable a time-series measurement of choroidal
39
40 322 oxygenation. Any faulty image frame or eye-blinks could also be easily identified and removed
41
42 323 from the data. Previous protocols [20, 21] that have used the reflection intensity, which was
43
44 324 directly recorded onto a photodiode with the corrections employed in the present study, would
45
46 325 not have been possible. The other advantage of the technique presented here is that it can be
47
48 326 used to image both eyes simultaneously, although the data presented in figures 5, 6 and 7 are
49
50 327 based on images from one pupil only.
51
52
53
54
55
56
57
58
59
60

1
2
3 328 While increased oxygen tension has considerable constrictive effect on retinal vessels, such
4
5 329 effect is minor in the choroid. The morphological effect of oxygen tension on the choroid is
6
7
8 330 minimal to none and choroidal vasoconstriction unlikely to influence OD. Previous studies on
9
10 331 choroidal and retinal oxygen saturation using the Oxymap T1 device support this [22].
11
12
13 332 While using the fundus ODR for calculating oxygen saturation, it is important to know which
14
15 333 region of the fundus (and underlying choroid) is being sampled. The process depends mainly
16
17 334 on the direction of gaze as described earlier in section 3.1. The effect of direction of the gaze
18
19 335 on fundus ODR was also assessed (Figure 4). It is important that when using fundus reflections
20
21 336 for oximetry purposes, to sample a constant region of the fundus and to avoid imaging the optic
22
23 337 disc. Consequently, only the macula region was illuminated during pupil reflection
24
25 338 experiments. Furthermore the avascular nature of the macular region means the sampled region
26
27 339 is dominated by choroidal blood.
28
29
30
31
32 340 In this study, we have demonstrated proof-of-principle recording in dark conditions. Future
33
34 341 work will refine the technique for use in ambient light by employing calibration and correction
35
36 342 of the reflection of ambient light from a calibration surface and the use of alternatives to a
37
38 343 calibration tile for calibration – for example, the sclera can also serve as an approximate
39
40 344 calibration. Reflection of ambient light from the retina is negligible compared to the reflection
41
42 345 of the flash illumination and can be neglected.
43
44
45
46
47 346 We have successfully demonstrated in human subjects that fundus ODR is capable of detecting
48
49 347 changes in blood oxygenation and that these measures correspond to changes observed using
50
51 348 pulse oximetry suggesting that the ODR can be used to calculate choroidal oxygenation. For
52
53 349 all the subjects, ODR decreased from an average value of 1.7 (\pm 0.4) to 1.3 (\pm 0.4) during the
54
55 350 period of inhaling the hypoxic gas mixture which tracked the changes in pulse oximeter values
56
57 351 from 97 (\pm 0.5) % to 86 (\pm 2) %. Thus we have demonstrated the ability to measure intra-
58
59
60

subject changes in blood oxygenation, the large inter-subject variability is due to differences in retinal pigment epithelial layer between subjects. These differences indicate that for absolute oximetry a process of calibration would be required for each subject. Future work should aim to understand and reduce this inter-subject variability. One way to characterise the fundus and choroidal pigmentation could be to record the iris and skin colour and estimate the choroidal pigmentation based on these characteristics [40].

The results described in this study were based on a small number of subjects ($n = 10$). A study based on a larger number of subjects that comprises individuals with a range of iris and skin colour would be useful to determine the degree of variability across a more general population.

There are certain advantages from using fundus reflection oximetry over retinal oximetry. A good quality retinal image is crucial to perform retinal oximetry which requires proper imaging technique and training. In contrast, fundus reflection images are relatively easy to acquire. Retinal oximetry image analysis is a lengthy and complex process when compared to fundus reflection oximetry. The other unique advantage is that unlike retinal oximetry, fundus reflection oximetry could be performed in both the eyes simultaneously.

The method we present involves co-axial illumination and spectral imaging of pupils, exploiting the spectral signature applied to light emitted from the pupil following two-way transmission through the choroid. Although it is similar to the work of Broadfoot et al[20] and Laing et al[21], these researchers employed techniques that are essentially non imaging and time sequential; they utilised modified ophthalmoscopes to focus light reflected from the fundus, through the pupil onto single photodetectors. In contrast, we have imaged the pupil to record the light reflected by the ocular fundi at multiple wavelengths in a single snapshot. This apparatus has enabled remote (~ 90 mm standoff) assessment of choroidal oxygenation and demonstrates that, in principle; oximetry at large standoff ranges is also possible. The technique

1
2
3 376 has possible applications for remote triage in emergency medicine or systemic blood oximetry
4
5 377 in for example sport or high-stress activities or in scenarios where pulse oximeter is limited
6
7
8 378 e.g. motion artefacts, low pulse problem, pigmentation, and poor perfusion (due to cold, shock,
9
10 379 sepsis or heart attack). Furthermore, this technique could be adapted for simultaneous imaging
11
12 380 of both eyes which opens the possibility of temporally-resolved bilateral discrimination of
13
14 381 ocular disparity and systemic oximetry effects.
15
16
17
18 382 Measurement of Choroidal-oxygen saturation could provide a viable surrogate measurement
19
20 383 of oxygen saturation in the cerebral vasculature. Such an approach could be useful in
21
22 384 understanding the pathophysiology of diseases such as age-related macular degeneration[13,
23
24 385 14], diabetic retinopathy[15, 16] in which choroidal blood flow plays an important role [22].
25
26
27 386 Other potential application includes blood loss and internal bleeding assessment in trauma
28
29 387 victims. Using this technique, we may also detect arrival of a de-saturation signal from the
30
31 388 lungs to the blood circulation of both the eyes, a technique that could potentially be useful in
32
33 389 detecting carotid artery stenosis.
34
35
36
37 390 In conclusion, the particular advantage of the technique presented in this pilot study on ten
38
39 391 healthy individuals is the standoff sensing of the oxygenation of blood in the choroidal
40
41 392 circulation as a proxy for systemic and cerebral oxygenation. We have demonstrated a
42
43 393 measurement precision of 0.5% for short-term changes in blood oxygenation. We have
44
45 394 employed relatively high-cost laboratory equipment that was available to us, however the
46
47 395 technique could be readily implemented using low cost mass-produced cameras and, for
48
49 396 example, LED illumination.
50
51
52
53

54 397 **References**

56 398 1. Wise, G.N., C.T. Dollery, and P. Henkind, *The retinal circulation*. 1971, New York: Harper &
57 399 Row.
58 400 2. Birol, G., et al., *Oxygen distribution and consumption in the macaque retina*. American Journal
59 401 of Physiology - Heart and Circulatory Physiology, 2007. **293**(3): p. H1696-H1704.

3. Tachibana, H., F. Gotoh, and Y. Ishikawa, *Retinal vascular autoregulation in normal subjects*. Stroke, 1982. **13**(2): p. 149-55.
4. Alm, A. and A. Bill, *Blood Flow and Oxygen Extraction in the Cat Uvea at Normal and High Intraocular Pressures*. Acta Physiologica Scandinavica, 1970. **80**(1): p. 19-28.
5. Hardarson, S.H., et al., *Automatic Retinal Oximetry*. Investigative Ophthalmology & Visual Science, 2006. **47**(11): p. 5011-5016.
6. Hammer, M., et al., *Retinal vessel oximetry-calibration, compensation for vessel diameter and fundus pigmentation, and reproducibility*. Journal of Biomedical Optics, 2008. **13**(5): p. 054015-054015-7.
7. Beach, J.M., et al., *Oximetry of retinal vessels by dual-wavelength imaging: calibration and influence of pigmentation*. Journal of Applied Physiology, 1999. **86**(2): p. 748-758.
8. Choudhary, T.R., et al., *Assessment of Acute Mild Hypoxia on Retinal Oxygen Saturation Using Snapshot Retinal Oximetry*. Investigative Ophthalmology & Visual Science, 2013. **54**(12): p. 7538-7543.
9. Blumenroder, S., A.J. Augustin, and F.H. Koch, *The influence of intraocular pressure and systemic oxygen tension on the intravascular pO₂ of the pig retina as measured with phosphorescence imaging*. Surv Ophthalmol, 1997. **42 Suppl 1**: p. S118-26.
10. Wilson, D.F., et al., *Oxygen distribution and vascular injury in the mouse eye measured by phosphorescence-lifetime imaging*. Applied optics, 2005. **44**(25): p. 5239-5248.
11. Linsenmeier, R.A., et al., *Retinal hypoxia in long-term diabetic cats*. Invest Ophthalmol Vis Sci, 1998. **39**(9): p. 1647-57.
12. Ahmed, J., et al., *Oxygen distribution in the macaque retina*. Investigative Ophthalmology & Visual Science, 1993. **34**(3): p. 516-521.
13. Pournaras, C.J., et al., *Regulation of Subfoveal Choroidal Blood Flow in Age-Related Macular Degeneration*. Investigative Ophthalmology & Visual Science, 2006. **47**(4): p. 1581-1586.
14. Friedman, E., *A hemodynamic model of the pathogenesis of age-related macular degeneration*. American journal of ophthalmology, 1997. **124**(5): p. 677-682.
15. Nagaoka, T., et al., *Alteration of choroidal circulation in the foveal region in patients with type 2 diabetes*. British Journal of Ophthalmology, 2004. **88**(8): p. 1060-1063.
16. Schocket, L.S., et al., *Foveolar choroidal hemodynamics in proliferative diabetic retinopathy*. International ophthalmology, 2004. **25**(2): p. 89-94.
17. Langham, M.E., et al., *Choroidal blood flow in diabetic retinopathy*. Experimental Eye Research, 1991. **52**(2): p. 167-173.
18. Roher, A.E., et al., *Cerebral blood flow in Alzheimer's disease*. Vascular Health and Risk Management, 2012. **8**: p. 599-611.
19. Mazza, M., et al., *Primary cerebral blood flow deficiency and Alzheimer's disease: shadows and lights*. J Alzheimers Dis, 2011. **23**(3): p. 375-89.
20. Broadfoot, K.D., J. Gloster, and D.P. Greaves, *Photoelectric method of investigating the amount and oxygenation of blood in the fundus oculi*. British Journal of Ophthalmology, 1961. **45**(3): p. 161-182.
21. Laing, R.A., L.A. Danisch, and L.R. Young, *The choroidal eye oximeter: an instrument for measuring oxygen saturation of choroidal blood in vivo*. Biomedical Engineering, IEEE Transactions on, 1975(3): p. 183-195.
22. Kristjansdottir, J.V., et al., *Choroidal Oximetry With a Noninvasive Spectrophotometric Oximeter*. Investigative Ophthalmology & Visual Science, 2013. **54**(5): p. 3234-3239.
23. Elsner, A.E., et al., *Reflectometry with a scanning laser ophthalmoscope*. Applied Optics, 1992. **31**(19): p. 3697-3710.
24. Hunold, W. and P. Malessa, *[Spectrophotometric determination of melanin pigmentation of the human fundus oculi]*. Ber Zusammenkunft Dtsch Ophthalmol Ges, 1974. **72**: p. 246-50.
25. Delori, F.C. and K.P. Pflibsen, *Spectral reflectance of the human ocular fundus*. Applied Optics, 1989. **28**(6): p. 1061-1077.

1
2
3
4
5
6
7
8
9
10
11
12
13
14
15
16
17
18
19
20
21
22
23
24
25
26
27
28
29
30
31
32
33
34
35
36
37
38
39
40
41
42
43
44
45
46
47
48
49
50
51
52
53
54
55
56
57
58
59
60

26. Augsten, R., et al., *Nonproliferative diabetic retinopathy-reflection spectra of the macula before and after laser photocoagulation*. Ophthalmologica, 1998. **212**(2): p. 105-11.

27. Cooper, R.L., R.H. Eikelboom, and C.J. Barry, *Correlations between densitometry of red-free photographs and reflectometry with the scanning laser ophthalmoscope in normal subjects and glaucoma patients*. Int Ophthalmol, 1992. **16**(4-5): p. 243-6.

28. Eikelboom, R.H., R.L. Cooper, and C.J. Barry, *An improved method of densitometry of red-free retinal nerve fibre layer photographs*. Aust N Z J Ophthalmol, 1993. **21**(4): p. 219-26.

29. Berendschot, T.T., P.J. DeLint, and D. van Norren, *Fundus reflectance--historical and present ideas*. Prog Retin Eye Res, 2003. **22**(2): p. 171-200.

30. Hammer, M., et al., *Optical properties of ocular fundus tissues-an in vitro study using the double-integrating-sphere technique and inverse Monte Carlo simulation*. Physics in Medicine and Biology, 1995. **40**(6): p. 963-978.

31. Watkins, R. *OpticStudio models of the human eye*. 2013; Available from: <https://customers.zemax.com/os/resources/learn/knowledgebase/zemax-models-of-the-human-eye>.

32. Gorman, A., D.W. Fletcher-Holmes, and A.R. Harvey, *Generalization of the Lyot filter and its application to snapshot spectral imaging*. Optics Express, 2010. **18**(6): p. 5602-5608.

33. Alabboud, I., et al., *New spectral imaging techniques for blood oximetry in the retina*. Proc. SPIE 6631, Novel Optical Instrumentation for Biomedical Applications III., 2007: p. 66310L-66310L.

34. Mordant, D.J., et al., *Spectral imaging of the retina*. Eye, 2011. **25**(3): p. 309-320.

35. Mordant, D.J., et al., *Validation of human whole blood oximetry, using a hyperspectral fundus camera with a model eye*. Invest Ophthalmol Vis Sci, 2011. **52**(5): p. 2851-9.

36. MacKenzie, L.E., et al., *In vivo oximetry of human bulbar conjunctival and episcleral microvasculature using snapshot multispectral imaging*. Experimental Eye Research.

37. Harvey, A.R., et al. *Technology options for imaging spectrometry*. 2000.

38. Beach, J.M., et al., *Oximetry of retinal vessels by dual-wavelength imaging: calibration and influence of pigmentation*. J Appl Physiol (1985), 1999. **86**(2): p. 748-58.

39. Spurling, K.J., C. Zammit, and S. Lozewicz, *Mains-powered hypoxic gas generation: a cost-effective and safe method to evaluate patients at risk from hypoxia during air travel*. Thorax, 2011. **66**(8): p. 731-732.

40. Franssen, L., J.E. Coppens, and T.J.T.P. van den Berg, *Grading of Iris Color with an Extended Photographic Reference Set*. Journal of Optometry, 2008. **1**(1): p. 36-40.

Appendix

Here we show that there is a linear relationship between the Optical Density Ratio (ODR) and blood oxygen saturation (s). Our fundamental measurement is of the average intensity of light at the detector corresponding to the radiance at the calibration tile and at the pupil at two wavelengths. If we assume the calibration tile to be Lambertian, then the output of a detector pixel in the image of the tile is given by

$$v_c = \eta A^\lambda \pi L_o^\lambda N_i^2 \tag{1}$$

where A^λ is the albedo of the tile, L_o^λ is the irradiance in the plane of the tile and pupil due to the light source, N_i is numerical aperture of the entrance aperture of the imaging system and η is a conversion factor taking into account the responsivity of the detector and the image-space numerical aperture of the imaging system. The total optical power illuminating the retina through the pupil is therefore $a_p L_o^\lambda$ where a_p is the area of the pupil. For simplicity, we will assume that this light is scattered by the sclera with two-way transmission through the choroid and attenuated according to the Beer-Lambert law. We also assume that the light intensity illuminating the pupil due to illumination by the retinal reflection is uniform (although we observe departures from this approximation). To a good approximation the scattering by the calibration tile is Lambertian and the irradiance at the pupil is independent of the illumination distribution at the retina and is therefore equal to $a_p L_o^{\lambda_1} / 2\pi r^2$ where r is the radius of the eye. As shown in Figure 2, all light from the illuminated area of the retina that exits the pupil is transmitted through the pupil; that is the light reflected back through the pupil is not Lambertian and so the output of a pixel corresponding to an image of the pupil is

$$v_p = \frac{\eta a_p L_o^\lambda}{2\pi r^2} 10^{-2\varepsilon^\lambda cl} \quad (2)$$

where the exponential term corresponds to application of the Beer-Lambert law, ε^λ is the extinction coefficient of blood at wavelength λ and l is the thickness of the choroid. The ODR for measurements recorded at wavelengths λ_1 and λ_2 is therefore given by

$$ODR = \frac{\log_{10} \frac{v_p^{\lambda_1}}{v_c^{\lambda_1}}}{\log_{10} \frac{v_p^{\lambda_2}}{v_c^{\lambda_2}}} = \frac{\xi^{a_p, \lambda_1} - \varepsilon^{\lambda_1} cl}{\xi^{a_p, \lambda_2} - \varepsilon^{\lambda_2} cl}, \quad (3)$$

where

$$\xi^{a,\lambda} = \log_{10} \left(\frac{a}{2A^\lambda (r\pi N_i)^2} \right) \quad (4)$$

We employ spectrally neutral calibration tiles so $A^{\lambda_1} = A^{\lambda_2}$ and due to mydriasis a can be assumed constant during the experiments and $\xi^{a,\lambda}$ can be considered as a constant, ξ . Taking the log of ratio of $v_p^{\lambda_1} / v_c^{\lambda_1}$ to $v_p^{\lambda_2} / v_c^{\lambda_2}$ yields

$$cl = \frac{OD^{\lambda_1} - OD^{\lambda_2}}{\epsilon^{\lambda_2} - \epsilon^{\lambda_1}}, \quad (5)$$

which can be substituted into (6) to yield

$$\epsilon^{\lambda_2} = \epsilon^{\lambda_1} \frac{OD^{\lambda_2} - \xi}{OD^{\lambda_1} - \xi}. \quad (6)$$

We choose λ_2 to be an isosbestic point, such as 800 nm, and λ_1 to be an oxygen-sensitive wavelength such as 780 nm and substitute $\epsilon^{\lambda_1} = s\epsilon_{HbO}^{\lambda_1} + (1-s)\epsilon_{Hb}^{\lambda_1}$, where s is optical saturation and the subscripts HbO and Hb denote the extinction coefficients for oxygenated and deoxygenated haemoglobin respectively there is a proportionate relationship between s and ODR:

$$s = \frac{1}{\epsilon_{HbO}^{780} - \epsilon_{Hb}^{780}} \left(\epsilon^{\lambda_2} \frac{OD^{780} - \xi}{1 - \frac{\xi}{OD^{800}}} - \epsilon_{HbO}^{\lambda_1} \right) \quad (7)$$

$$= m.ODR + c$$

where

$$m = \frac{\epsilon^{\lambda_2}}{(\epsilon_{HbO}^{780} - \epsilon_{Hb}^{780}) \left(1 - \frac{\xi}{OD^{800}} \right)} \quad (8)$$

$$c = -\frac{\epsilon^{\lambda_2}}{\epsilon_{HbO}^{780} - \epsilon_{Hb}^{780}} \left(\frac{\xi}{OD^{800} - \xi} + \frac{\epsilon_{HbO}^{\lambda_1}}{\epsilon^{\lambda_2}} \right) \quad (9)$$

1
2
3 529 Note that ξ varies with a_p and so both the gradient and offset of this relationship are sensitive
4
5
6 530 to variations in the pupil diameter.
7
8
9
10
11
12
13
14
15
16
17
18
19
20
21
22
23
24
25
26
27
28
29
30
31
32
33
34
35
36
37
38
39
40
41
42
43
44
45
46
47
48
49
50
51
52
53
54
55
56
57
58
59
60